



Coupling $\text{Nd}^{3+}:\text{Y}_2\text{O}_3$ fluorescent submicron particles to linear plasmonic chains

D. Hernández-Pinilla^a, N. Nogal^a, L. Sánchez-García^a, S. Carretero-Palacios^a,
K. de Oliveira Lima^{b,c}, A. Ferrier^{b,d}, P. Goldner^b, L.E. Bausá^{a,e}, M.O. Ramírez^{a,e,*}

^a Dept. Física de Materiales and Instituto de Ciencia de Materiales Nicolás Cabrera, Universidad Autónoma de Madrid, 28049, Madrid, Spain

^b Chimie ParisTech, PSL University, CNRS, Institut de Recherche de Chimie Paris, 75005, Paris, France

^c Laboratório de Materiais Luminescentes Micro e Nanoestruturados-Mater Lumen, Departamento de Química, Faculdade de Filosofia, Ciências e Letras de Ribeirão Preto, Universidade de São Paulo, Ribeirão Preto, 14040-900, São Paulo, Brazil

^d Faculté des Sciences et Ingénierie, Sorbonne Université, UFR 933, 75005, Paris, France

^e Condensed Matter Physics Center (IFIMAC), Universidad Autónoma de Madrid, 28049, Madrid, Spain

ABSTRACT

We report on the fabrication and optical characterization of a new hybrid material consisting of Nd^{3+} doped Y_2O_3 submicron particles associated with linear chains of plasmonic nanostructures. By drop-casting deposition, single Nd^{3+} doped Y_2O_3 polycrystalline particles are dispersed and located in the vicinities of plasmonic chains of silver nanoparticles formed on the surface a LiNbO_3 substrate. The interaction between the plasmonic modes of the chain with the fluorescent yttria submicron particles is analyzed by micro-luminescence experiments. Orthogonal polarization configurations of the excitation radiation, namely, perpendicular and parallel to plasmonic chain axis, are employed to study the effect of the longitudinal and transverse chain plasmonic modes on the luminescence of the particles. A remarkable dependence of the emission intensity of the $\text{Nd}^{3+}:\text{Y}_2\text{O}_3$ submicron particles on the excitation polarization is observed, showing the capability of plasmonic chains to modulate the emission of fluorescent submicron particles in contact with the chain. Numerical simulations evidence a different distribution of the excitation radiation field within the $\text{Nd}^{3+}:\text{Y}_2\text{O}_3$ particle depending on the type of excited plasmonic mode, longitudinal or transversal, of the chain, and hence, the ability of plasmonic chains for controlling the emission of Rare Earth doped submicron particles.

1. Introduction

Since the last decades, trivalent Rare Earth (RE) doped nano and submicron particles are the subject of intense attention due to their adaptability and performance in photonic applications such as bio-imaging [1] or solid-state lighting [2]. More recently, RE doped materials are also being considering for optical quantum information processing applications [3–5]. Due to the shielding by the outer 5s and 5p electrons, the intra 4f–4f transitions of trivalent RE ions lead to very narrow optical homogeneous linewidths, while spin transitions with long coherence lifetimes are also available. This feature is of great relevance in quantum technologies, and indeed, rare earth doped bulk crystal are among the most promising systems for quantum storage communications [6].

However, the need to integrate RE doped materials as e.g. solid-state single photon emitters on a photon chip, and the control of the optical features by coupling the emitting ion to nanocavities motivates the study of low dimensional RE doped materials [7,8]. In this context, recent works have reported the advantages of RE doped Y_2O_3 nanocrystals as

potential platforms for quantum technologies owing to their remarkable optical and spin coherence properties, narrow size distribution and other bulk-like optical properties [9]. Moreover, RE doped Y_2O_3 ceramics possess several outstanding properties such as an excellent thermal stability and a high refractive index useful for light confinement and manipulation [10]. These features make this system a highly desirable platform for a wide range of applications including optoelectronics and photonics. In particular, Nd^{3+} doped Y_2O_3 has demonstrated favorable properties as solid state lasers, active waveguides and nano-thermometers due to its good stability and transparency in a wide spectral region [10–13].

In this work, we present the fabrication and characterization of a new hybrid material consisting of Nd^{3+} doped Y_2O_3 submicron particles associated with plasmonic nanostructures to explore the possibility of coupling between those types of systems. As plasmonic nanostructures, long chains formed by closely spaced Ag nanoparticles (NPs) are employed. The use of this plasmonic chains has been revealed as a promising strategy for the manipulation and control of the RE ion emission at the nanoscale. In fact, the emergence of new functionalities

* Corresponding author. Condensed Matter Physics Center (IFIMAC), Universidad Autónoma de Madrid, 28049, Madrid, Spain.

E-mail address: mariola.ramirez@uam.es (M.O. Ramírez).

<https://doi.org/10.1016/j.jlumin.2023.120220>

Received 15 June 2023; Received in revised form 18 September 2023; Accepted 21 September 2023

Available online 27 September 2023

0022-2313/© 2023 The Authors. Published by Elsevier B.V. This is an open access article under the CC BY-NC-ND license (<http://creativecommons.org/licenses/by-nc-nd/4.0/>).

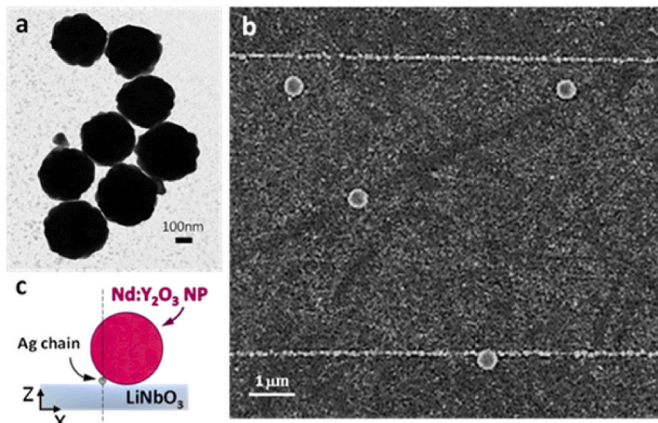


Fig. 1. a) TEM image of an aggregate of as-synthesized round-shaped $\text{Nd}^{3+}:\text{Y}_2\text{O}_3$ submicron particles. b) SEM image of $\text{Nd}^{3+}:\text{Y}_2\text{O}_3$ submicron particles after dispersion and drop casting on the surface of a periodically poled LN crystal on which Ag NP chains were previously formed by ferroelectric lithography. Well-dispersed single particles are obtained, either isolated or in the vicinity of the plasmonic Ag chain. c) Schematics of the configuration used in the numerical simulations representing the plasmonic chain along the y axis on top of the LN substrate, together with a spherical $\text{Nd}^{3+}:\text{Y}_2\text{O}_3$ particle located at a side, and tangent to the Ag chain. The indicated X-Z plane at the midplane of the Ag NP chain corresponds to the cross-sectional view shown in the simulations.

such as nanolasing [14–16], the control of the spatial coherence of the RE emitters [17], or the subwavelength fluorescence guiding at ultra-long distances [18] have been demonstrated when Ag NP chains are deposited on top of RE doped macroscopic bulk crystals.

Here, Nd^{3+} doped Y_2O_3 submicron particles are located in close proximity to linear chains of silver NPs which have been deposited onto a LiNbO_3 substrate (hereafter LN). The refractive index of the LN substrate (around 2.2 in the spectral range of interest) is larger than that of the Y_2O_3 (around 1.9) [19], which makes it possible to couple the excitation radiation from the substrate into the fluorescent particles through their point contact, providing the main mechanism of optical excitation of the RE ion into the yttria system. Additionally, the use of LN is of current technological interest as an outstanding and versatile platform to develop a wide variety of integrated photonic devices [20–22].

The work is organized as follows. First, the morphology of the Y_2O_3 submicron particles and their distribution onto the LN substrate in the vicinity of the Ag plasmonic chains is presented by means of transmission and scanning electron microscopy images. Then, we show the main optical properties of the different components forming the hybrid system. To investigate the effect of the plasmonic chains on the $\text{Nd}^{3+}:\text{Y}_2\text{O}_3$ particles, confocal micro-fluorescence experiments for different polarization configurations of the excitation radiation were carried out to analyze the emission of $\text{Nd}^{3+}:\text{Y}_2\text{O}_3$ in the proximity of the plasmonic chains. Finally, the experimental data are complemented with representative results from numerical simulations to attain a qualitative physical insight of the coupling process taking place. The work evidences the possibility of controlling the emission of the $\text{Nd}^{3+}:\text{Y}_2\text{O}_3$ submicron particles by means of the coupling and the reorganization of the excitation field distribution inside the fluorescent system using plasmonic NP chains. The results constitute a promising step on the search for controlling and coupling novel RE based nanoscale devices by means of plasmonic nanostructures on a technologically relevant platform.

2. Material and methods

2.1. Sample preparation

Nd^{3+} doped Y_2O_3 submicron particles were prepared by homogeneous precipitation. We used $\text{Y}(\text{NO}_3)_3 \cdot 6\text{H}_2\text{O}$ (99.9% pure, Alfa Aesar) and $\text{Nd}(\text{NO}_3)_3 \cdot 6\text{H}_2\text{O}$ (99.99% pure, Reacton) as yttrium and neodymium sources. For the synthesis, an appropriate amount of urea ($\text{CO}(\text{NH}_2)_2 > 99\%$ pure, Sigma) was dissolved in a mixed Nd/Y aqueous nitrate solution and heated at 85°C for 24 h. The employed concentrations were 0.5 mol L^{-1} and 7.5 mmol L^{-1} for urea and metals (Nd^{3+} and Y^{3+}), respectively. After annealing of this precursor at 1200°C for 6 h, 2 at% $\text{Nd}^{3+}:\text{Y}_2\text{O}_3$ particles (cubic phase, $\text{Ia}\bar{3}$ space group) of about 400 nm were obtained. Their polycrystalline structure was evidenced by transmission electron microscopy (see Fig. 1a) in agreement with previous works. More details on the preparation procedure and the structural characterization can be found in ref. 23.

Linear chains of Ag NPs were prepared on the domain boundaries surfaces of a periodically-poled LN crystal substrate following a cost-effective photo-deposition process commonly known as ferroelectric lithography [24]. Briefly, the plasmonic chains were formed by immersing the LN crystal in a 0.01 M AgNO_3 solution at 65°C while illuminating the surface with UV radiation at 254 nm. Additional information on the fabrication process of silver NP chains can be found elsewhere [25].

Finally, to locate the Nd^{3+} doped Y_2O_3 submicron particles in the vicinity of the linear chains of silver NPs, drop-casting deposition method was employed. Specifically, a drop of a homogeneous dispersed solution of 2% $\text{Nd}^{3+}:\text{Y}_2\text{O}_3$ in ethanol 0.005 M, was deposited onto the LN substrate containing the silver NP chains, and dried with a Nitrogen flow.

2.2. Characterization of $\text{Nd}:\text{Y}_2\text{O}_3$ and Ag plasmonic chains

TEM images of the as-synthesized $\text{Nd}^{3+}:\text{Y}_2\text{O}_3$ submicron particles were acquired with a JEOL 1010 transmission electron microscope operating at 100 kV. The $\text{Nd}^{3+}:\text{Y}_2\text{O}_3$ particles dispersed onto the LN substrate and the photo-deposited Ag NP chains were characterized by scanning electron microscopy (SEM) using a Philips XL30 field emission gun scanning electron microscope. Transmission optical microscopy was employed to obtain the main absorption features of $\text{Nd}^{3+}:\text{Y}_2\text{O}_3$ submicron particles in the visible spectral range.

Micro-fluorescence experiments were carried out in a customized Olympus BX41 laser scanning confocal microscope controlled by LabSpec 5 Spectroscopy software (Horiba). The 488 nm spectral line of an Ar^+ laser was used as excitation source and focused on the sample by a 100x MPlan FLN Olympus microscope objective (NA = 0.9). The emitted light was collected through the same objective lens in backscattering geometry. The detection module consisted of an iHR 550 monochromator (Horiba) connected to a Peltier-cooled Horiba CCD (Synapse model).

2.3. Numerical simulations

The optical properties of an Ag NP chain, in combination with a single Y_2O_3 submicron particle, on top of a LN substrate, were calculated using the Ansys Lumerical FDTD commercial software. The simulation was performed in a 3D FDTD box with dimensions of $1612 \times 4000 \times 5000 \text{ nm}^3$ along the x, y, and z directions. To ensure accurate results, an auto-nonuniform mesh with an accuracy of 3 and a conformal variant 0 mesh refinement type were utilized. Symmetry and periodic boundary conditions were applied along the x and y directions, respectively. For the z-axis, stretched coordinate perfect-matching layers (PML) with 64 layers and a standard profile were employed. The system was illuminated by a plane wave illumination source propagating in air along the z direction. Both parallel- and perpendicular-polarizations to the

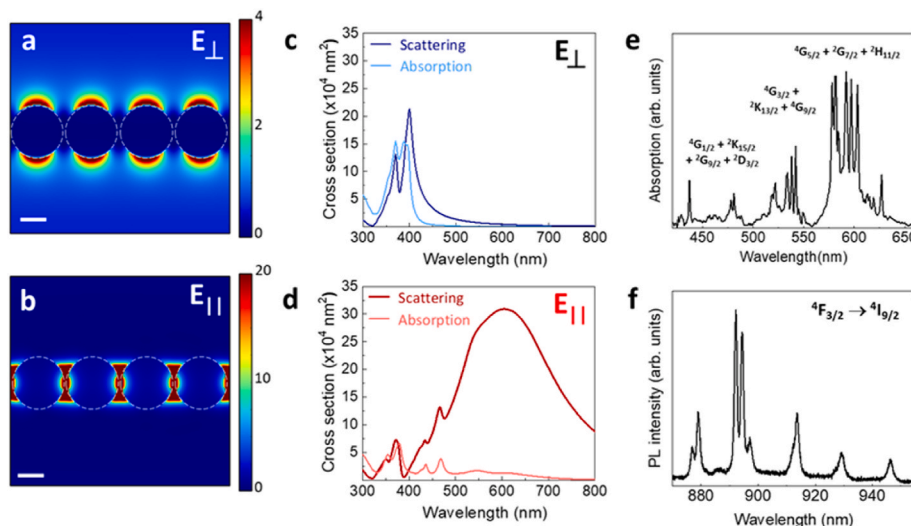


Fig. 2. Spatial distribution of the near field at the midplane of a plasmonic chain consisting of Ag NPs of 50 nm diameter and a 2 nm gap between them for an incident plane wave at $\lambda = 535$ nm (a) perpendicular and (b) parallel to the chain. The scale bar corresponds to 25 nm. Simulation of the far-field absorption (light line) and scattering (dark line) spectra of the Ag NP chain for an incident plane wave polarized (c) perpendicular and (d) parallel to the chain. e) Absorption spectrum of Nd³⁺:Y₂O₃ submicron particles in the 440–600 nm spectral range. Relevant transitions are indicated. f) Emission spectrum of the Nd³⁺:Y₂O₃ submicron particles corresponding to the $^4F_{3/2} \rightarrow ^4I_{9/2}$ Nd³⁺ transition.

plasmonic chain axis were analyzed to fully characterize the system's response. The chain consisted of 31 spherical silver NPs with a diameter of 50 nm and a 2 nm gap between them. The optical constants of the nanoparticles were fitted to the provided bulk permittivity data in ref [26]. The chain was placed on top of a LN substrate with a refractive index of $n_{LN} = 2.2$. Additionally, a spherical Y₂O₃ particle with a diameter of 500 nm and a refractive index of $n_{Y_2O_3} = 1.93$ was positioned on the substrate in the vicinity of the plasmonic chain. The Y₂O₃ particle was placed at a side, and tangent to the Ag NP chain to investigate their interaction.

3. Results and discussion

A TEM image of the as-synthesized Nd³⁺:Y₂O₃ submicron particles is shown in Fig. 1a. As observed, after the synthesis route, aggregates of quasi-spherical polycrystalline Nd³⁺:Y₂O₃ particles, with an average diameter of around 400 nm, were obtained. Fig. 1b shows a SEM image obtained after dispersion and drop-casting, to place Nd³⁺:Y₂O₃ NPs onto the LN substrate after the formation of the linear chains of Ag nanoparticles by the photo-deposition process. These chains exhibit a millimeter length, being the average size of the Ag NPs close to 50 nm with an interspacing distance of around 2 nm [14]. As can be seen, a suitable spatial distribution is achieved to study the interaction between the Nd³⁺:Y₂O₃ submicron particles and the Ag NP chains. Indeed, single Nd³⁺:Y₂O₃ submicron particles can be found in close proximity of the plasmonic chains, as well as isolated from them. Finally, Fig. 1c shows the schematic of the position of the Y₂O₃ particle with respect to the Ag NP chain, which has been used in the numerical simulations: the particle is located on one side of the plasmonic chain touching it tangentially.

With regards to the optical properties, Fig. 2 presents the response of the different components forming the hybrid system (namely, Ag NP chain and Nd³⁺:Y₂O₃ submicron particles), in the relevant spectral region. Fig. 2a and b shows the results of the numerical simulation of the near field amplitude at a wavelength of 535 nm, close to the experimental excitation wavelength, computed in the proximity of an isolated plasmonic chain. The simulations were performed for plane waves polarized both parallel and perpendicular to the chain axis. The contour plot, taken at the midplane of the nanoparticles, clearly illustrates the significant field enhancement occurring in the gap between the particles when the polarization is parallel to the chain. In this configuration, the

electric field intensity reaches the highest values due to the plasmonic coupling between adjacent nanoparticles. Conversely, when the polarization is perpendicular to the chain, the pattern resembles that of individual nanoparticles, exhibiting a different field distribution with significant lower values of the field intensity. These results align with previous reports on the near field response of this type of chain in the 0.8–1 μ m spectral region [14,15], confirming the enhanced field localization and coupling effects in the parallel configuration, while the perpendicular configuration retains characteristics similar to isolated nanoparticles. The far field plasmonic response supported by the chains at both orthogonal polarizations is displayed in Fig. 2c and d. Both panels include the calculated absorption and scattering cross-section spectra when the electric field is polarized parallel and perpendicular to the chain axis, hence exciting the longitudinal and transverse plasmonic modes, respectively. As observed, when the transverse mode is excited, the plasmonic resonance is centered around 400 nm featuring similar absorption and scattering values (Fig. 2c). However, the excitation of the longitudinal mode results into a much broader resonance, which extends from the visible down to the near infrared region with its maximum centered at around 600 nm. It also exhibits a remarkable intensity difference between the absorption and scattering cross-section values. This feature, along with the negligible dissipation losses in the NIR spectral region has been exploited for the enhancement and polarization control of several optical processes [27] and is of particular significance in the context of this research, as it overlaps the most relevant Nd³⁺ absorption and emission transitions used during the photoluminescence experiments.

The optical absorption in the visible spectral region and the near infrared $^4F_{3/2} \rightarrow ^4I_{9/2}$ emission of as-synthesized Nd³⁺:Y₂O₃ submicron particles are displayed in Fig. 2e and f, respectively. In both spectra the observed Nd³⁺ Stark transitions are in good agreement with previously reported data on the spectroscopy properties of Nd³⁺ in Y₂O₃ polycrystalline ceramics, confirming the bixbyite cubic structure of our particles [11,28,29]. In this crystal structure, Nd³⁺ ions substitute for Y³⁺ ions at both C₂ and C_{3i} symmetry sites. While Nd³⁺ at C_{3i} sites yield intrinsically weak magnetic dipole transitions, Nd³⁺ ions at C₂ symmetry sites show forced electric dipole transitions, which are mainly responsible of the observed transition lines in our spectra. In principle, Nd³⁺ at C₂ symmetry sites should lead to polarization sensitive Nd³⁺ transitions. However, the cubic and polycrystalline character of the

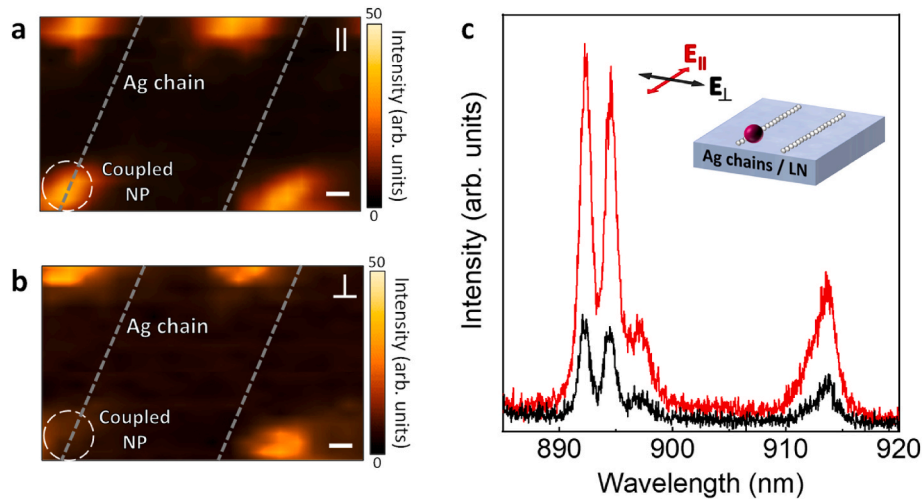


Fig. 3. Spatial distribution of the integrated emission intensity associated with the $^4F_{3/2} \rightarrow ^4I_{9/2}$ transition of Nd^{3+} in Y_2O_3 submicron particles located onto the LN substrate for excitation radiation polarized a) parallel and b) perpendicular to the axis chain. Ag chains are represented in gray dashed lines. The $\text{Nd}^{3+}:\text{Y}_2\text{O}_3$ submicron particle located in close contact to an Ag chain is highlighted by a dashed circle. The scale bar corresponds to 500 nm. c) Polarized emission spectrum of the highlighted $\text{Nd}^{3+}:\text{Y}_2\text{O}_3$ particle in close contact to an Ag chain.

synthesized $\text{Nd}^{3+}:\text{Y}_2\text{O}_3$ submicron particles lead to polarization-insensitive optical spectra even for single particles, as confirmed in our experiments.

The interaction between $\text{Nd}^{3+}:\text{Y}_2\text{O}_3$ submicron particles and the localized plasmon modes supported by linear plasmonic chains was studied by means of spatially resolved confocal spectroscopy. Orthogonal polarization configurations of the excitation radiation, namely,

perpendicular and parallel to Ag chain axis, were employed to assess the possibility of coupling the different plasmonic modes to the fluorescent particles. For the experiments, the excitation wavelength was fixed at 488 nm as it spectrally overlaps the transversal and the longitudinal modes sustained by the chain, and at the same time allows the optical excitation of Nd^{3+} ions into the yttria host (see Fig. 2). Polarization-driven modifications in emitted intensity are analyzed and compared

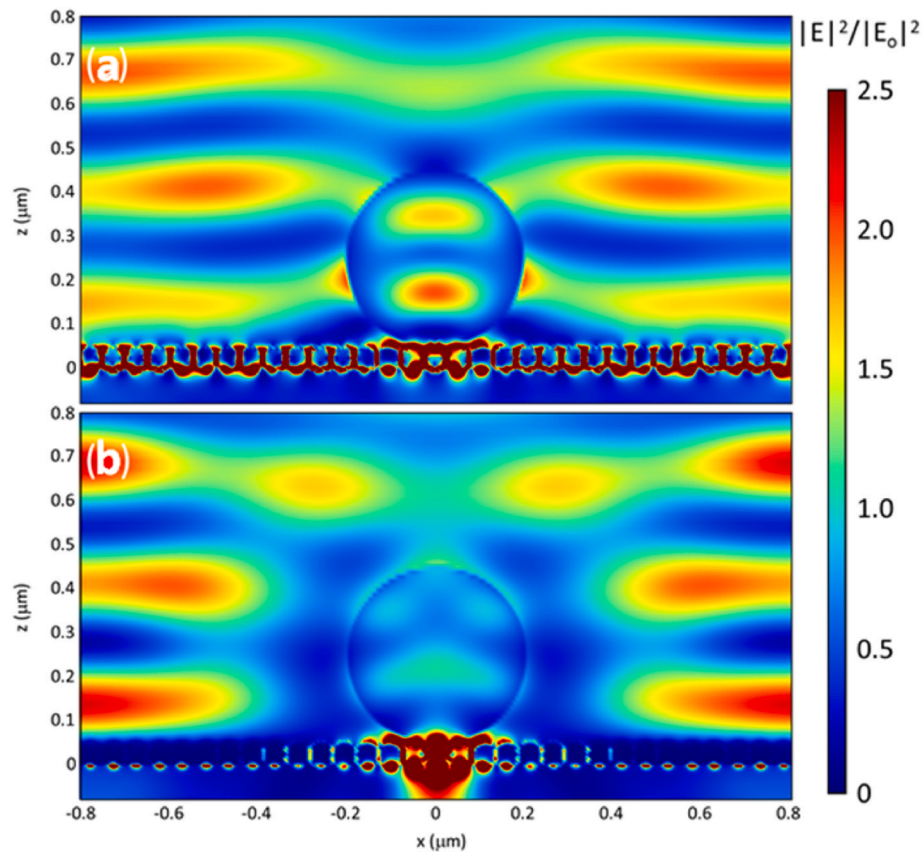


Fig. 4. a) Simulations of the spatial distribution of the electric field in the vicinities of a $\text{Nd}^{3+}:\text{Y}_2\text{O}_3$ submicron particle in close contact to an Ag chain for an incident plane wave of $\lambda = 535$ nm polarized a) parallel and b) perpendicular to the Ag chain axis. The simulation corresponds to a cross-sectional view of the transversal x-z plane at the midplane of the Ag NP chain as sketched in Fig. 1c.

with uncoupled isolated submicron particles through their fluorescence spectra to evaluate how the near field excitation of the plasmonic chain modes can be employed to manipulate and control the emission properties of RE doped submicron particles in close proximity. Spatial distributions of the integrated ${}^4F_{3/2} \rightarrow {}^4I_{9/2}$ emission of $\text{Nd}^{3+}:\text{Y}_2\text{O}_3$ particles obtained from the surface of the hybrid system under excitation polarized parallel (top) and perpendicular (bottom) to the plasmonic chains direction are shown in Fig. 3a and b. The comparison between both images shows that the emitted intensity arising from $\text{Nd}^{3+}:\text{Y}_2\text{O}_3$ particles localized far from the plasmonic chains remain unchanged regardless the polarization state of the excitation radiation, in agreement with their cubic and polycrystalline nature [23]. However, when the fluorescent yttria submicron particle is in contact with the plasmonic chain, a remarkable dependence on the excitation polarization is observed. Specifically, the total emitted intensity recorded from the $\text{Nd}^{3+}:\text{Y}_2\text{O}_3$ submicron particle significantly decreases when the excitation beam is polarized perpendicular to the chain axis. These results reveal the capability of plasmonic chains to modulate the emitted intensity depending on the type of plasmonic mode, longitudinal or transversal, interacting with the submicron yttria particle. Fig. 3c displays the emission spectra registered for the coupled particle upon parallel (red) and perpendicular (black) excitation. As observed, a substantial intensity reduction by a factor of ~ 3 is achieved when exciting the transverse plasmonic chain mode. These results point towards a dominant effect of the plasmonic chain on the coupling and field distribution of excitation light inside the submicron particles. In fact, the obtained results contrast with those reported for RE doped bulk crystals in association with plasmonic nanostructures. While selective photoluminescence enhancement of Stark transitions with a specific polarization character has been demonstrated by plasmonic resonances for Nd^{3+} in bulk crystals [30,31], to our knowledge, this work reports for the first time the use of plasmonic chain modes to control unpolarized emission of RE-doped polycrystalline submicron particles.

To have a first qualitative explanation about the optical response of the hybrid system, numerical simulations were carried out to explore the effects of the interaction between the plasmonic chain and the Y_2O_3 submicron particle. A simple model consisting of a single Y_2O_3 spherical particle with a diameter of 500 nm, located on top of the LN substrate, adjacent to a plasmonic chain has been considered. Specifically, the Y_2O_3 submicron particle is situated on one side of the chain, touching it tangentially (Fig. 1c). Fig. 4 illustrates the intensity distribution of the electric field under illumination with a plane wave at a wavelength of 535 nm along the z direction for polarizations parallel and perpendicular to the plasmonic chain. The figure represents a cross-sectional view in the x-z plane, taken at the midplane of the Ag NPs chain (see Fig. 1c). Only a portion of the Y_2O_3 particle is visible in the figure (rather than its complete diameter) since the plane of intersection between the Y_2O_3 particle and the chain is not aligned with the diameter of the yttria particle. In agreement with the findings depicted in Fig. 2, the parallel illumination configuration leads to notable field enhancement between the gaps of the plasmonic Ag NP chain (see Fig. 4a).

In addition, for this configuration, it is particularly intriguing the presence of high-intensity lobes within the Y_2O_3 submicron particle under parallel illumination. In this case, the presence of the plasmonic chain clearly enables the coupling of light inside the Y_2O_3 sphere at the excitation wavelength of Nd^{3+} , in agreement with the experimental observations. Conversely, when the illumination is perpendicular to the chain (see Fig. 4b), the enhancement between the Ag NP gaps vanishes and the near field radiation is mainly concentrated at the point contact between the plasmonic chain and the yttria host, outside of this particle. Consequently, the coupling of the excitation radiation into the Y_2O_3 submicron particle is remarkably lower than that observed in the parallel configuration, in agreement with the experimental observations shown in Fig. 3. Accordingly, the results of the simulations point towards a different coupling efficiency of the excitation radiation into the yttria particle, which would explain well the experimental results on the

emission intensity, depending on the linear polarization state with respect to the plasmonic chain orientation. In fact, the reorganization of the excitation field distribution within the $\text{Nd}^{3+}:\text{Y}_2\text{O}_3$ submicron particle due to the presence of the plasmonic chain provides a means for controlling the emission of the Nd doped yttria particle.

To summarize, we have shown that linear chains of closely spaced interacting plasmonic nanoparticles can strongly influence the excitation, and hence the emission properties of fluorescent $\text{Nd}^{3+}:\text{Y}_2\text{O}_3$ submicron particles in contact with the chain. As compared with isolated particles, changing the linear polarization state of the excitation beam results in a strong reduction of the emitted intensity attributable to the redistribution of the excitation field inside the fluorescence particles when excited via the transverse plasmonic chain mode by light linearly polarized perpendicular to the chain axis. The results constitute a previous step to exploit the sub-diffractive waveguides properties of plasmonic chains as a mean to control the emission of fluorescent particles. In addition, the use of a technologically relevant platform for integrated on-chip photonic devices opens alternative pathways to obtain all polarization switchable devices by taking advantage of the anisotropic optical response of the linear arrangements operating at the nanoscale.

Declaration of competing interest

The authors declare that they have no known competing financial interests or personal relationships that could have appeared to influence the work reported in this paper.

Data availability

Data will be made available on request.

Acknowledgements

This work has been supported by the Spanish State Research Agency under contracts PID2019-108257GB-I00, PID2022-137444NB-I00 and the María de Maeztu “Programme for Units of Excellence in R&D” CEX2018-000805-M. P.G acknowledges funding from the French Agence Nationale de la Recherche under grant ANR-20-CE09-0022 (UltraNanOSpec). The authors acknowledge the contribution of Beatriz H. Juárez on the dispersion of the fluorescence submicron particles and the TEM images.

References

- [1] Y. Liu, Y. Lu, X. Yang, X. Zheng, S. Wen, F. Wang, X. Vidal, J. Zhao, D. Liu, Z. Zhou, C. Ma, J. Zhou, J.A. Piper, P. Xi, D. Jin, Amplified stimulated emission in upconversion nanoparticles for super-resolution nanoscopy, *Nature* 543 (2017) 229–233, <https://doi.org/10.1038/nature21366>.
- [2] M.H. Fang, J.L. Leano, Jr, R.S. Liu, Control of narrow-band emission in phosphor materials for application in light-emitting diodes, *ACS Energy Lett.* 3 (10) (2018) 2573–2586, <https://doi.org/10.1021/acsenenergylett.8b01408>.
- [3] W. Tittel, M. Afzelius, T. Chanelière, R.L. Cone, S. Kröll, S.A. Moiseev, M. Sellars, Photon-echo quantum memory in solid state systems, *Laser Photonics Rev.* 4 (2010) 244–267, <https://doi.org/10.1002/lpor.200810056>.
- [4] A. Lvovsky, B. Sanders, W. Tittel, Optical quantum memory, *Nat. Photonics* 3 (2009) 706–714, <https://doi.org/10.1038/nphoton.2009.231>.
- [5] C. Clausen, I. Usmani, F. Bussi eres, N. Sangouard, M. Afzelius, H. De Riedmatten, N. Gisin, Quantum storage of photonic entanglement in a crystal, *Nature* 469 (2011) 508–511, <https://doi.org/10.1038/nature09662>.
- [6] D. Lago-Rivera, S. Grandi, J.V. Rakonjac, A. Seri, H. de Riedmatten, Telecommunication heralded entanglement between multimode solid-state quantum memories, *Nature* 594 (2021) 37, <https://doi.org/10.1038/s41586-021-03481-8>.
- [7] T. Zhong, J.M. Kindem, J.G. Bartholomew, J. Rochman, I. Craiciu, V. Verma, S. W. Nam, F. Marsili, M.D. Shaw, A.D. Beyer, A. Faraon, Optically addressing single rare-earth ions in a nanophotonic cavity, *Phys. Rev. Lett.* 121 (2018), 183603, <https://doi.org/10.1103/PhysRevLett.121.183603>.
- [8] A.M. Dibos, M. Raha, C.M. Phenice, J.D. Thompson, Atomic source of single photons in the telecom band, *Phys. Rev. Lett.* 120 (2018), 243601, <https://doi.org/10.1103/PhysRevLett.120.243601>.
- [9] T. Zhong, P. Goldner, Emerging rare-earth doped material platforms for quantum nanophotonics, *Nanophotonics* 8 (11) (2019) 2003–2015, <https://doi.org/10.1515/nanoph-2019-0185>.

- [10] J. Lu, J. Lu, T. Murai, K. Takaichi, T. Uematsu, K. Ueda, H. Yagi, T. Yanagitani, A. Kaminskii, $\text{Nd}^{3+}:\text{Y}_2\text{O}_3$ ceramic laser, *Jpn. J. Appl. Phys.* 40 (2001) L1277–L1279, <https://doi.org/10.1143/JJAP.40.L1277>.
- [11] B.M. Walsh, J.M. McMahon, W.C. Edwards, N.P. Barnes, R.W. Equall, R. L. Hutcheson, Spectroscopic characterization of $\text{Nd}:\text{Y}_2\text{O}_3$: application toward a differential absorption lidar system for remote sensing of ozone, *J. Opt. Soc. Am. B* 19 (2002) 2893–2903, <https://doi.org/10.1364/JOSAB.19.002893>.
- [12] N. Dong, Y. Yao, F. Chen, J.R.V. de Aldana, Channel waveguides preserving luminescence features in $\text{Nd}^{3+}:\text{Y}_2\text{O}_3$ ceramics produced by ultrafast laser inscription, *Phys. Status Solidi RRL* 5 (2011) 184–186, <https://doi.org/10.1002/pssr.201105166>.
- [13] N. Rakov, Y. Xing, G.S. Maciel, Optical thermometry Operation within all three biological windows using $\text{Nd}^{3+}:\text{Er}^{3+}:\text{Y}_2\text{O}_3$ nanocomposite phosphors, *ACS Appl. Nano Mater.* 3 (10) (2020) 10479–10486, <https://doi.org/10.1021/acsnanm.0c02397>.
- [14] P. Molina, E. Yraola, M. O. Ramírez, C. Tserkezis, J.L. Plaza, J. Aizpurua, J. Bravo-Abad, L.E. Bausá, Plasmon-Assisted Nd^{3+} -based solid-state nanolaser, *Nano Lett.* 16 (2016) 895–899, <https://doi.org/10.1021/acs.nanolett.5b03656>.
- [15] D. Hernández-Pinilla, P. Molina, C. de las Heras, J. Bravo-Abad, L.E. Bausá, M. O. Ramírez, Multiline, Operation from a single plasmon-assisted laser, *ACS Photonics* 5 (2) (2018) 406–412, <https://doi.org/10.1021/acsp Photonics.7b00846>.
- [16] L. Sánchez-García, M. O. Ramírez, R.M. Solé, J.J. Carvajal, F. Díaz, L.E. Bausá, Plasmon-induced dual-wavelength operation in a Yb^{3+} laser, *Light Sci. Appl.* 8 (1) (2019) 14, <https://doi.org/10.1038/s41377-019-0125-2>.
- [17] J. Fernández-Martínez, S. Carretero-Palacios, L. Sánchez-García, J. Bravo-Abad, P. Molina, N. van Hoof, M. O. Ramírez, J. Gómez-Rivas, L.E. Bausá, Spatial coherence from Nd^{3+} quantum emitters mediated by a plasmonic chain, *Opt Express* 29 (16) (2021), 26244, <https://doi.org/10.1364/OE.433080>.
- [18] J. Fernández-Martínez, S. Carretero-Palacios, P. Molina, J. Bravo-Abad, M. O. Ramírez, L.E. Bausá, Silver nanoparticle Chains for ultra-long-range plasmonic Waveguides for Nd^{3+} fluorescence, *Nanomaterials* 12 (2022) 4296, <https://doi.org/10.3390/nano12234296>.
- [19] Y. Nigara, Measurement of the optical constants of yttrium oxide, *Jpn. J. Appl. Phys.* 7 (1968) 404, <https://doi.org/10.1143/JJAP.7.404>.
- [20] D. Sun, Y. Zhang, D. Wang, W. Song, X. Liu, J. Pang, D. Geng, Y. Sang, H. Liu, Microstructure and domain engineering of lithium niobate crystal films for integrated photonic applications, *Light Sci. Appl.* 9 (2020) 197, <https://doi.org/10.1038/s41377-020-00434-0>.
- [21] D. Zhu, L. Shao, M. Yu, R. Cheng, B. Desiatov, C.J. Xin, Y. Hu, J. Holzgrafe, S. Ghosh, A. Shams-Ansari, E. Puma, N. Sinclair, C. Reimer, M. Zhang, M. Lončar, Integrated photonics on thin-film lithium niobate, *Adv. Opt. Photon* 13 (2021) 242–352, <https://doi.org/10.1364/AOP.411024>.
- [22] Y. Qi, Y. Li, Integrated lithium niobate photonics, *Nanophotonics* 9 (6) (2020) 1287–1320, <https://doi.org/10.1515/nanoph-2020-0013>.
- [23] K. de Oliveira Lima, R. Rocha Gonçalves, D. Giaume, A. Ferrier, P. Goldner, Influence of Defects on sub- μm optical Linewidths in $\text{Eu}^{3+}:\text{Y}_2\text{O}_3$ particles, *J. Lumin.* 168 (2015) 276, [10.1016/j.jlumin.2015.07.009](https://doi.org/10.1016/j.jlumin.2015.07.009).
- [24] S. Kalinin, D. Bonnell, T. Alvarez, X. Lei, Z. Hu, R. Shao, J. Ferris, Ferroelectric lithography of multicomponent nanostructures, *Adv. Mater.* 16 (2004) 795–799, <https://doi.org/10.1002/adma.200305702>.
- [25] E. Yraola, P. Molina, J.L. Plaza, M. O. Ramírez, L.E. Bausá, Spontaneous Emission and nonlinear response Enhancement by silver Nanoparticles in a Nd^{3+} -doped periodically poled LiNbO_3 laser crystal, *Adv. Mater.* 25 (2013) 910–915, <https://doi.org/10.1002/adma.201203176>.
- [26] M.J. Weber, *Handbook of Optical Materials*, CRC Press, New York, 2003, <https://doi.org/10.1201/9781315219615>.
- [27] M. O. Ramírez, P. Molina, A. Gómez-Tornero, D. Hernández-Pinilla, L. Sánchez-García, S. Carretero-Palacios, L.E. Bausá, Hybrid plasmonic-ferroelectric architectures for lasing and SHG processes at the nanoscale, *Adv. Mater.* 31 (2019), 1901428, <https://doi.org/10.1002/adma.201901428>.
- [28] D.K. Sardar, D.M. Dee, K.L. Nash, R.M. Yow, J.B. Gruber, Optical absorption intensity analysis and emission cross sections for the intermanifold and the inter-Stark transitions of $\text{Nd}^{3+}(4f^3)$ in polycrystalline ceramic Y_2O_3 , *J. Appl. Phys.* 100 (12) (2016), 123106, <https://doi.org/10.1063/1.2402970>.
- [29] W. Liu, L. Jin, S. Wang, Preparation of ZrO_2 -doped $\text{Nd}^{3+}:\text{Y}_2\text{O}_3$ transparent ceramic and the corresponding characteristic of luminescence, *Mater. Chem. Phys.* 236 (2019), 121835, <https://doi.org/10.1016/j.matchemphys.2019.121835>.
- [30] E. Yraola, L. Sánchez-García, C. Tserkezis, P. Molina, M. O. Ramírez, J. Aizpurua, L. E. Bausá, Polarization-selective enhancement of Nd^{3+} photoluminescence assisted by linear chains of silver nanoparticles, *J. Lumin.* 169 (2016) 569, <https://doi.org/10.1016/j.jlumin.2014.12.053>.
- [31] P. Molina, E. Yraola, M.O. Ramírez, J. Plaza, C. de las Heras, L.E. Bausá, Selective Plasmon Enhancement of the $1.08\ \mu\text{m}$ Nd^{3+} Laser Stark Transition by Tailoring Ag Nanoparticles Chains on a Y-Cut PPLN, *Nano Lett.* 13 (2013) 4931–4936, <https://doi.org/10.1021/nl4028999>.